Hindawi
International Journal of Energy Research
Volume 2023, Article ID 9077811, 9 pages
https://doi.org/10.1155/2023/9077811

*Research Article*

# Enhanced Thermoelectric Performance of Lightly Pb-Doped $Sb_2Te_3$ Polycrystalline Alloys for Power Generation in Midtemperature Range

**Okmin Park,[1] Kyu Hyoung Lee,[2] Sang Jeong Park,[1] Se Woong Lee,[1] and Sang-il Kim[1]**

[1]*Department of Materials Science and Engineering, University of Seoul, Seoul 02504, Republic of Korea*
[2]*Department of Materials Science and Engineering, Yonsei University, Seoul 03722, Republic of Korea*

Correspondence should be addressed to Sang-il Kim; sang1.kim@uos.ac.kr

Received 7 July 2023; Revised 22 August 2023; Accepted 19 September 2023; Published 10 October 2023

Academic Editor: Nagaraj Nandihalli



$Sb_2Te_3$ alloys are promising thermoelectric materials because of their outstanding electrical transport properties in the midtemperature range of 500–700 K, while codoping with multiple elements has been successful to improve their thermoelectric performance. In this study, enhanced thermoelectric properties with a maximum thermoelectric figure of merit of 0.97 are reported for singly and lightly Pb-doped $Sb_2Te_3$ polycrystalline alloys ($Sb_{2-x}Pb_xTe_3$). Very light Pb doping in the range $0.005 \le x \le 0.0125$ in the $Sb_{2-x}Pb_xTe_3$ alloys yielded significantly improved carrier transport properties and increased electrical conductivity while the Seebeck coefficient is decreased moderately, since the density-of-state effective mass is improved much. As a result, power factor for the Pb-doped $Sb_2Te_3$ is largely increased up to 3.7 $mW/mK^2$ at 300 K. The lattice thermal conductivity decreased considerably owing to the additional point defect phonon scattering by the Pb despite slight doping. Consequently, a maximum thermoelectric figure of merit of 0.97 was obtained for $Sb_{1.9875}Pb_{0.0125}Te_3$ ($x = 0.0125$) at 600 K, which is the highest reported value for singly doped $Sb_2Te_3$-based alloys. A maximum energy conversion efficiency was calculated to be 9.0% for a temperature difference of 350 K, which is higher than that for other singly or codoped $Sb_2Te_3$ alloys.

## 1. Introduction

Thermoelectric materials have been attracting attention for solid-state cooling and energy harvesting because they can convert heat directly into electricity. Therefore, there exist many potential applications, including cryoprobes, on-chip cooling, and power generators based on waste heat from automobiles and industries [1–4]. However, the widespread applications of thermoelectric materials depend on their conversion efficiency, which is typically characterized by the thermoelectric figure of merit. The thermoelectric figure of merit is a dimensionless quantity given by $zT = S^2\sigma T/\kappa_{tot}$, where $S$, $\sigma$, $T$, and $\kappa_{tot}$ are the Seebeck coefficient, electrical conductivity, absolute temperature, and total thermal conductivity, respectively. Note that the average figure of merit ($zT_{avg}$) is an important measure of the power generation efficiency of a thermoelectric material over a temperature range. The maximum energy conversion efficiency ($\eta_{max}$) of a thermoelectric material can be estimated using the following equation:

$$\eta_{max} = \frac{\Delta T}{T_h}\frac{\sqrt{1+zT_{avg}}-1}{\sqrt{1+zT_{avg}}+(T_c/T_h)}, \quad (1)$$

where $T_c$ is the temperature of the cold side of the thermoelectric material, $T_h$ is the temperature of the hot side of the thermoelectric material, $\Delta T$ is $T_h - T_c$, and $T_{avg}$ is $(T_h + T_c)/2$.

$(Bi,Sb)_2Te_3$ solid solution alloys are the most widely used $p$-type thermoelectric materials at room temperature. In particular, Sb-rich alloys such as $Bi_{0.5}Sb_{1.5}Te_3$ and $Bi_{0.4}Sb_{1.6}Te_3$ are known to exhibit high $p$-type thermoelectric performance because of their optimized carrier transport

properties [5–7]. Pristine $Bi_2Te_3$ typically exhibits *n*-type electrical transport behavior; interestingly, when $Bi_2Te_3$ is alloyed with $Sb_2Te_3$, which exhibits *p*-type electrical transport properties, a high $\sigma$ of >2,000 S/cm can be obtained [8, 9]. Consequently, $(Bi,Sb)_2Te_3$ alloys can exhibit a high thermoelectric performance in the low-temperature range of 300–400 K. However, their performance degrades rapidly at higher temperatures owing to the occurrence of bipolar conduction, which is unfavorable for electric power generation [10]. In contrast, $Sb_2Te_3$ alloys demonstrate a high thermoelectric performance in the midtemperature range of 500–700 K, with no significant occurrence of bipolar conduction. Nevertheless, the maximum $zT$ of $Sb_2Te_3$ alloys is lower than that of $(Bi,Sb)_2Te_3$ alloys.

Several studies have been conducted to enhance the $zT$ of $Sb_2Te_3$ alloys in the midtemperature range. In particular, codoping $Sb_2Te_3$ with multiple elements has been shown to be successful [11–14]. For instance, Qin et al. reported a $zT$ of 1.0 at 673 K for $Sb_2Te_3$ codoped with Mn and In [12]; in addition, Hu et al. reported a maximum $zT$ of 0.92 at 710 K for $Sb_2Te_3$ codoped with In and Ag [13]. Moreover, a $zT$ of 0.96 at 680 K was reported for $Sb_2Te_3$ codoped with Mg and In [14]. However, $Sb_2Te_3$ has been typically shown to exhibit a high thermoelectric performance when codoped with two or more elements [15–18]. The maximum achievable $zT$ value for singly doped $Sb_2Te_3$ alloys is 0.7, which is significantly lower than that obtained via codoping [13, 19].

In this study, $Sb_2Te_3$ was doped with a single dopant, Pb, to enhance its thermoelectric performance. The performance of $(Bi,Sb)_2Te_3$ alloys has been shown to improve when Pb was used as an acceptor dopant [20–22]. To this end, a series of $Sb_{2-x}Pb_xTe_3$ alloys with $x = 0$, 0.0025, 0.005, 0.0075, 0.01, and 0.0125 was synthesized, where $x$ is the doping content. Pb doping significantly enhanced the power factor of the alloys, and a maximum $zT$ of 0.97 at 600 K was achieved for $x = 0.0125$ (i.e., $Sb_{1.9875}Pb_{0.0125}Te_3$). The thermoelectric properties of the $Sb_{2-x}Pb_xTe_3$ alloys were analyzed using various phenomenological parameters, including the density of state (DOS) effective mass ($m_d^*$) and weighted mobility ($\mu_w$). $m_d^*$ was found to increase linearly with the doping content, which in turn positively affected the thermoelectric performance of the $Sb_{2-x}Pb_xTe_3$ alloys. In addition, the further doping of Pb in $Sb_{2-x}Pb_xTe_3$ was investigated by introducing large amounts of Pb corresponding to $x = 0.05$, 0.1, 0.15, and 0.2 (Supplementary Information (available here)).

## 2. Experimental Methods

Polycrystalline $Sb_{2-x}Pb_xTe_3$ ($x = 0$, 0.0025, 0.005, 0.0075, 0.01, and 0.0125) samples were prepared using the traditional solid-state reaction method. Stoichiometric quantities of high purity Sb (99.999%; 5N Plus), Pb (99.999%; Alfa Aesar), and Te (99.999%; 5N Plus) were weighed according to the nominal composition of the desired alloy, placed in a quartz tube, and sealed under vacuum ($10^{-5}$ Torr). The sealed quartz ampoules were heated at 1,000 K for 4 h, and this temperature was further maintained for 6 h. Next, the ampoules were quenched in water at room temperature, following which the respective metal ingots were extracted from the ampoules. Ball milling (SPEX 8000D, Costa Mesa, USA) was performed in an Ar atmosphere to convert the ingots into powders. Subsequently, the powders were sintered at 573 K for 5 min at a pressure of 70 MPa under vacuum ($10^{-6}$ Torr) to form cylindrical bulk pellets using spark plasma sintering (SPS; SPS-1030, Sumitomo Coal Mining Co. Ltd., Tokyo, Japan). Note that the sintered bulk samples had a relative density of more than 99%.

The crystal structure of the samples was analyzed using X-ray diffraction (XRD; D8 Discover, Bruker, USA) with Cu–$K_{\alpha1}$ radiation. Atomic percentage of Pb dopant in the samples is measured using energy-dispersive spectroscopy (EDS, Quantax Xflash 6-60, Bruker, USA) by scanning electron microscope (SEM, SU8010, HITACHI, Japan). The $\sigma$ and $S$ values of the samples were measured using a thermoelectric property measuring system (ZEM-3M8, Advance Riko, Japan) in a He atmosphere between 300 and 650 K. The Hall measurements were conducted in the van der Pauw configuration at 300 K using a Hall measurement system (HMS-5300, Ecopia, Korea). A laser flash analyzer (LFA457, Netzsch, Germany) was used to obtain the thermal diffusivity ($\alpha$) of the samples, which was used to calculate $\kappa_{tot} = \alpha\rho C_p$, where $\rho$ and $C_p$ are the density and specific heat capacity of the sample, respectively. $\rho$ was measured (relative density of ≥97%), while $C_p = 0.2053$ J/g·K was used based on previously reported data [23]. The results corresponding to high Pb doping (i.e., $x \geq 0.05$) are presented in the Supplementary Information.

## 3. Results and Discussion

Figures 1(a) and 1(b) show the XRD patterns of the polycrystalline bulk $Sb_{2-x}Pb_xTe_3$ ($x = 0$, 0.0025, 0.005, 0.0075, 0.01, and 0.0125) samples obtained along the directions parallel (PA) and perpendicular (PE) to the sintering direction, respectively. The XRD patterns confirm the synthesis of different Pb-doped $Sb_2Te_3$ phases in accordance with the JCPDS#01-071-0393 card. The lattice parameters ($a$ and $c$) of the samples were calculated using the (015) and (1010) diffraction peaks. Figure 1(c) shows the lattice parameters as functions of $x$. The error bars indicate the measurement error of the diffraction data of Figures 1(a) and 1(b). The lattice parameter $a$ did not vary significantly with $x$, whereas the lattice parameter $c$ increased monotonically with $x$. This increase in $c$ with $x$ can be explained by the difference between the ionic radii of $Sb^{3+}$ (90 pm) and $Pb^{2+}$ (133 pm), which enables the successful doping of Pb at the Sb sites. In addition, Table 1 shows atomic ratio in $Sb_{2-x}Pb_xTe_3$ measured by EDS, and it was confirmed systematic increase in the amount of Pb (see Supplementary Information Figure S1 for EDS mapping). However, PbTe appeared as an impurity in the highly doped samples (i.e., $x \geq 0.05$; see Supplementary Information Figure S2(a)). This was further confirmed by the behavior of the corresponding lattice parameters with $x$ (see Supplementary Information Figure S2(b)).

Figures 2(a) and 2(e) show $\sigma$ as a function of temperature for the Pb-doped $Sb_2Te_3$ samples along the PE and PA directions, respectively. $\sigma$ of the $Sb_{2-x}Pb_xTe_3$ samples increased with $x$ along both the PE and PA directions. The

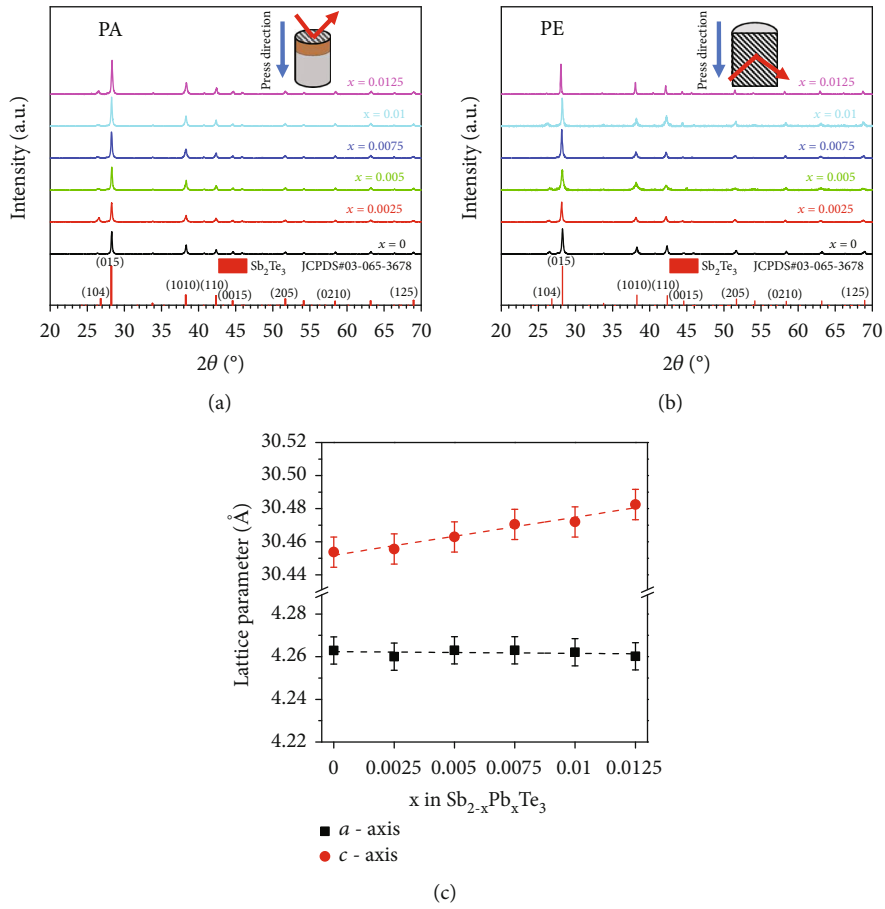


FIGURE 1: XRD patterns of the $Sb_{2-x}Pb_xTe_3$ samples for different doping content along (a) PA and (b) PE directions. (c) Lattice parameters as functions of doping content.

TABLE 1: Atomic percentage in $Sb_{2-x}Pb_xTe_3$ samples obtained from energy-dispersive spectroscopy (EDS).

| $Sb_{2-x}Pb_xTe_3$ | $x = 0$ | $x = 0.0025$ | $x = 0.005$ | $x = 0.0075$ | $x = 0.01$ | $x = 0.0125$ |
|---|---|---|---|---|---|---|
| Sb (at.%) | 41.39 | 41.20 | 41.20 | 40.77 | 41.11 | 41.17 |
| Te (at.%) | 58.61 | 58.73 | 58.68 | 59.07 | 58.67 | 58.56 |
| Pb (at.%) | — | 0.07 | 0.12 | 0.16 | 0.22 | 0.27 |

$\sigma$ values at 300 K along the PE direction were 2,240, 2,440, 2,620, 3,080, 3,570, and 3,770 S/cm for $x = 0$, 0.0025, 0.005, 0.0075, 0.01, and 0.0125, respectively, whereas the $\sigma$ values at 300 K along the PA direction were 1,640, 1,870, 2,020, 2,370, 2,430, and 2,730 S/cm for $x = 0$, 0.0025, 0.005, 0.0075, 0.01, and 0.0125, respectively. For the highly doped samples ($x \geq 0.05$), there was a sharp increase in $\sigma$, which had values in the range 5000–6000 S/cm; however, $\sigma$ decreased with a further increase in $x$ owing to the formation of secondary PbTe phases in these samples (see Supplementary Information; Figure S3(a)). This decrease in $\sigma$ with an increase in the doping content is because of the relatively low $\sigma$ of the PbTe phase of approximately 120–200 S/cm [24, 25].

Figures 2(b) and 2(f) show $S$ as a function of temperature for the $Sb_{2-x}Pb_xTe_3$ samples along the PE and PA directions, respectively. $S$ increased with temperature for all the samples. The $S$ value for $x = 0.0025$ was slightly higher than that for $x = 0$; however, for $x \geq 0.005$, $S$ decreased with $x$ along both the measured directions. Compared to the relatively large increase in $\sigma$ with $x$ (Figures 2(a) and 2(e)), the decrease in $S$ with $x$ was less significant. However, with further Pb doping (i.e., $x \geq 0.05$), $S$ decreased significantly, reaching a minimum value of 30 $\mu$V/K (see Supplementary Information Figure S3(b)). Figures 2(c) and 2(g) show the calculated power factor of the $Sb_{2-x}Pb_xTe_3$ samples as a function of temperature along the PE and PA directions, respectively. The power factor of the Pb-doped samples was significantly higher than that of pristine $Sb_2Te_3$ across the entire temperature range. A maximum power factor of 3.66 mW/mK$^2$ was obtained for $x = 0.01$ at 300 K along the PE direction, which is 39% higher than that for $x = 0$. A maximum power factor of 2.75 mW/mK$^2$ was obtained for $x = 0.01$ along the PA direction, which is 40% higher than that for $x = 0$ (1.96 mW/mK$^2$). A gradual decrease in the power factor was observed with further doping (see Supplementary Information Figure S3(c)).

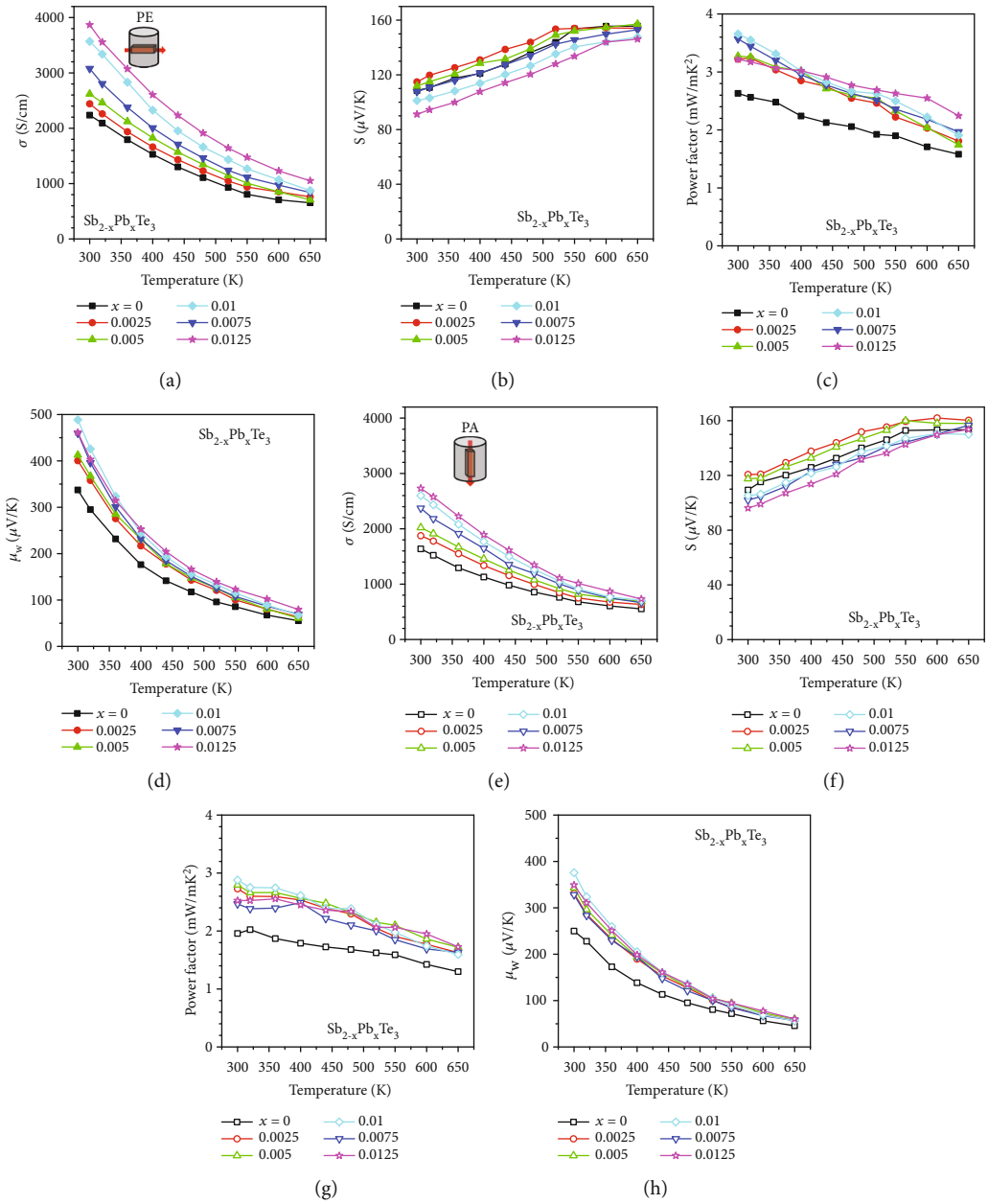


FIGURE 2: Thermoelectric transport properties of the $Sb_{2-x}Pb_xTe_3$ samples. (a, e) Electrical conductivity, (b, f) Seebeck coefficient, (c, g) power factor, and (d, h) weighted mobility, as functions of temperature along the PE and PA directions, respectively.

Figures 2(d) and 2(h) show $\mu_w$ as a function of temperature for the $Sb_{2-x}Pb_xTe_3$ samples along the PE and PA directions, respectively. $\mu_w$ is related to the maximum theoretical efficiency of a thermoelectric material and can be defined using the following analytical approximation of the Drude-Sommerfeld free-electron model for $|S| > 20\,\mu V/K$ [26]:

$$\mu_w = \frac{3h^3\sigma}{8\pi e(2m_e kT)^{3/2}}\left[\frac{\exp\left[(|S|/(k/e)) - 2\right]}{1+\exp\left[-5((|S|/(k/e)) - 1)\right]} + \frac{(3/\pi^2)(|S|/(k/e))}{1+\exp\left[5((|S|/(k/e)) - 1)\right]}\right], \quad (2)$$

where $h$ and $m_e$ denote Planck's constant and the electron mass, respectively. Note that $\mu_w$ is proportional to the maximum power factor of the sample, which can be obtained by optimizing the Hall carrier concentration $n_H$. In general, $\mu_w$ increased with the doping content along both the PE and PA directions. This confirms that the Pb-doped samples have enhanced electrical transport properties and hence can exhibit enhanced thermoelectric performance.

Figures 3(a) and 3(b) show $n_H$ and $\mu_H$ (along both the PE and PA directions) of the $Sb_{2-x}Pb_xTe_3$ samples as functions $x$ at 300 K. $n_H$ steadily increased with increasing Pb content and reached a maximum value of $1.16 \times 10^{20}\,cm^{-3}$ for $x = 0.0125$. By contrast, $\mu_H$ decreased

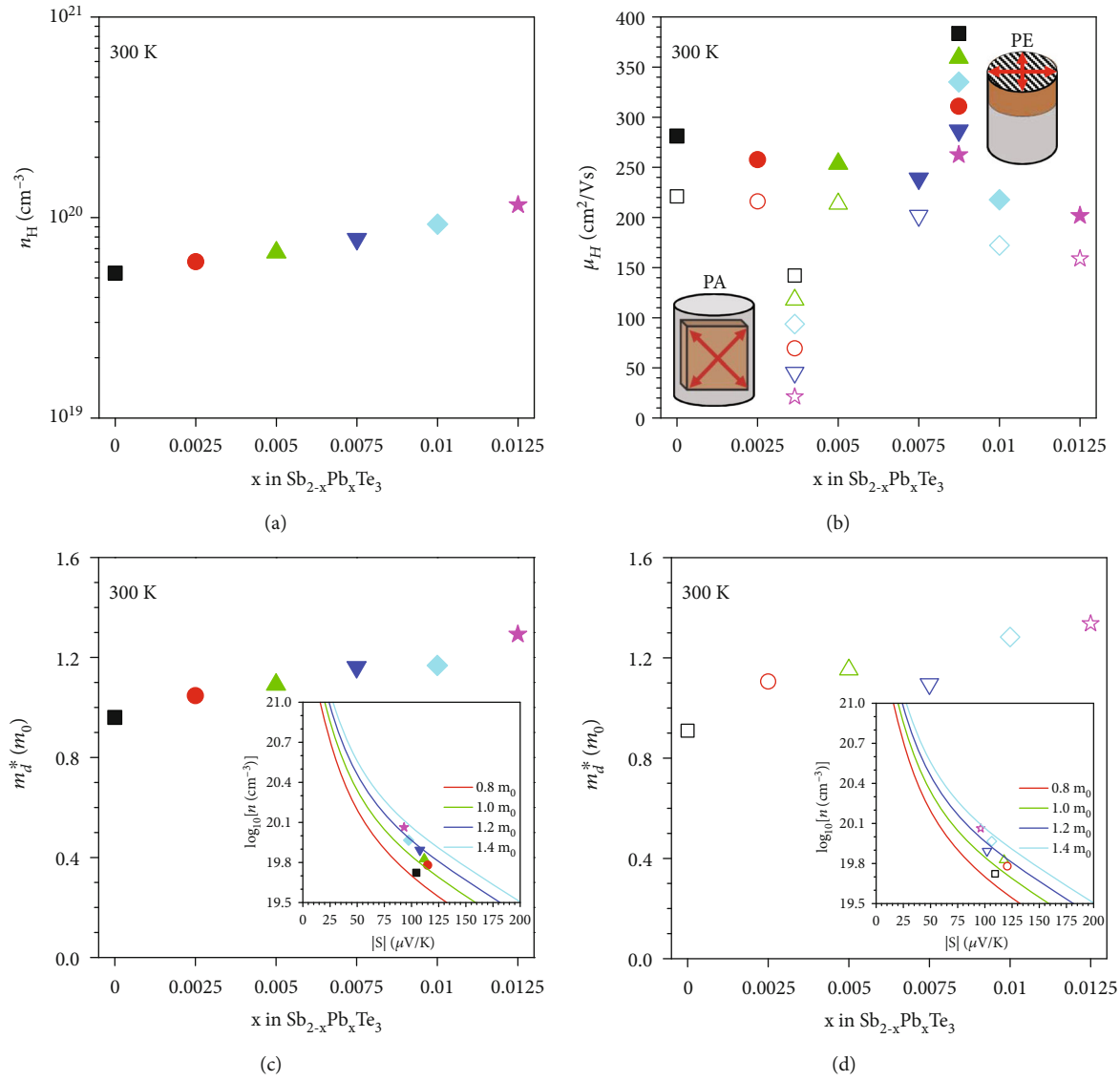


FIGURE 3: Carrier transport properties of the $Sb_{2-x}Pb_xTe_3$ samples. (a) Hall carrier concentration and (b) Hall mobility, as functions of doping content. DOS effective mass as a function of doping content along (c) PE and (d) PA directions. The insets in (c) and (d) show the logarithmic carrier concentration as a function of the absolute Seebeck coefficient along the PE and PA directions, respectively.

linearly with $x$ along both the measured directions. Moreover, $\mu_H$ along the PA direction was approximately 27% lower than that along the PE direction. The $\mu_H$ values along the PE direction were 281, 258, 254, 239, and 218 cm$^2$/Vs for $x = 0$, 0.0025, 0.005, 0.0075, 0.01, and 0.0125, respectively, whereas the $\mu_H$ values along the PA direction were 221, 216, 214, 202, and 172 cm$^2$/Vs for $x = 0$, 0.0025, 0.005, 0.0075, 0.01, and 0.0125, respectively. The increase in $\sigma$ with $x$ can be attributed to the increase in $n_H$ with $x$, which in turn is owing to the substitution of the $Sb^{3+}$ ions by the $Pb^{2+}$ ions. Supplementary Information Figure S4 presents the corresponding results of the highly doped samples.

The electrical transport properties of semiconductors are determined by the DOS at the Fermi level. The magnitude of the DOS is directly related to $m_d^*$. Thus, $m_d^*$ can be defined in terms of changes in the electron structure using the single parabolic band model [27], such that

$$\log_{10}\left(\frac{m_d^* T}{300}\right) = \frac{2}{3}\log_{10}(n) - \frac{2}{3}\left[20.3 - (0.00508 \times |S|) + \left(1.58 \times 0.967^{|S|}\right)\right]. \quad (3)$$

Figures 3(c) and 3(d) show $m_d^*$ of the $Sb_{2-x}Pb_xTe_3$ samples as a function of $x$ along the PE and PA directions, respectively. The insets in Figures 3(c) and 3(d) show $\log_{10}(n_H)$ as a function of $|S|$ for different samples, where the curves correspond to fixed $m_d^*$ values. $m_d^*$ increased with the Pb content along both the PE and PA directions, similar

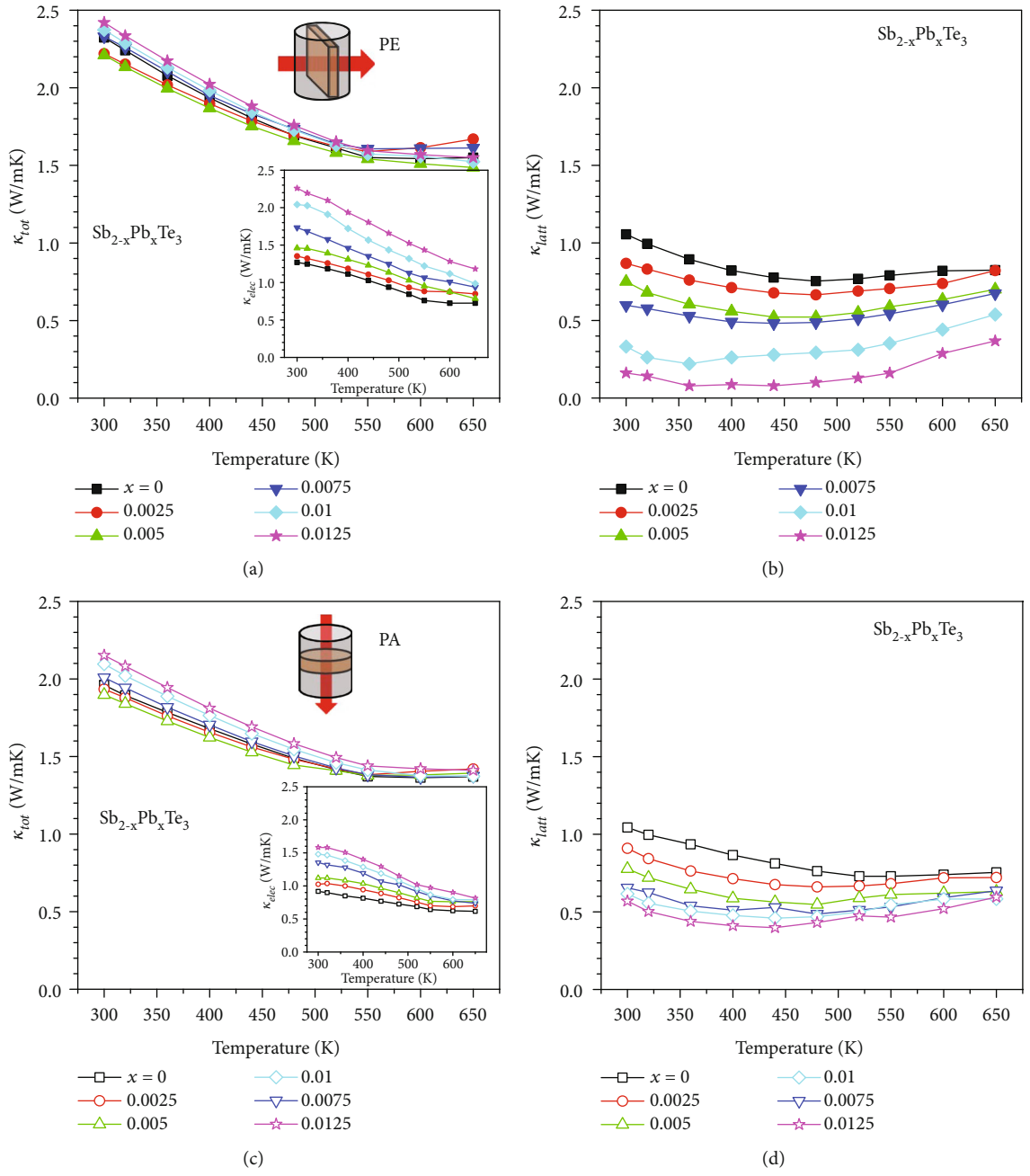


FIGURE 4: Thermal transport properties of the $Sb_{2-x}Pb_xTe_3$ samples. (a, c) Total thermal conductivity and (b, d) lattice thermal conductivity, as functions of temperature along the PE and PA directions, respectively. The insets in (a) and (c) show the electron thermal conductivity as a function of temperature along the PE and PA directions, respectively.

to $n_H$. The reason for this increase in $m_d^*$ with $x$ is that the rate of increase of $n_H$ with $x$ is faster than the rate of decrease of $|S|$ with $x$. The $m_d^*$ values at 300 K along the PE direction were 0.960, 1.05, 1.09, 1.16, 1.17, and 1.26 $m_0$ ($m_0$ being the rest mass of an electron) for $x = 0$, 0.0025, 0.005, 0.0075, 0.01, and 0.0125, respectively. $m_d^*$ along the PA direction also exhibited a similar trend. The maximum value of $m_d^*$ along the PA direction was 1.34 $m_0$ for $x =$ 0.0125. However, for $x > 0.05$, the $m_d^*$ value at 300 K decreased linearly with increasing doping content (Supplementary Information Figures S4(c) and (d)). For $x \geq 0.1$, $m_d^*$ of the highly doped samples was lower than that of pristine $Sb_2Te_3$.

Figure 4 shows $\kappa_{tot}$ and the lattice thermal conductivity $\kappa_{latt}$ of the $Sb_{2-x}Pb_xTe_3$ samples as functions of temperature along the PE and PA directions. $\kappa_{tot}$ of the Pb-doped samples varied nonmonotonically with $x$ along both the measured directions, as shown in Figures 4(a) and 4(c). The insets in Figures 4(a) and 4(c) show the electrical thermal conductivity $\kappa_{elec}$ of the $Sb_{2-x}Pb_xTe_3$ samples as a function of temperature, which was calculated using the Wiedemann-Franz law [28], namely, $\kappa_{elec} = L\sigma T$ (where $L$

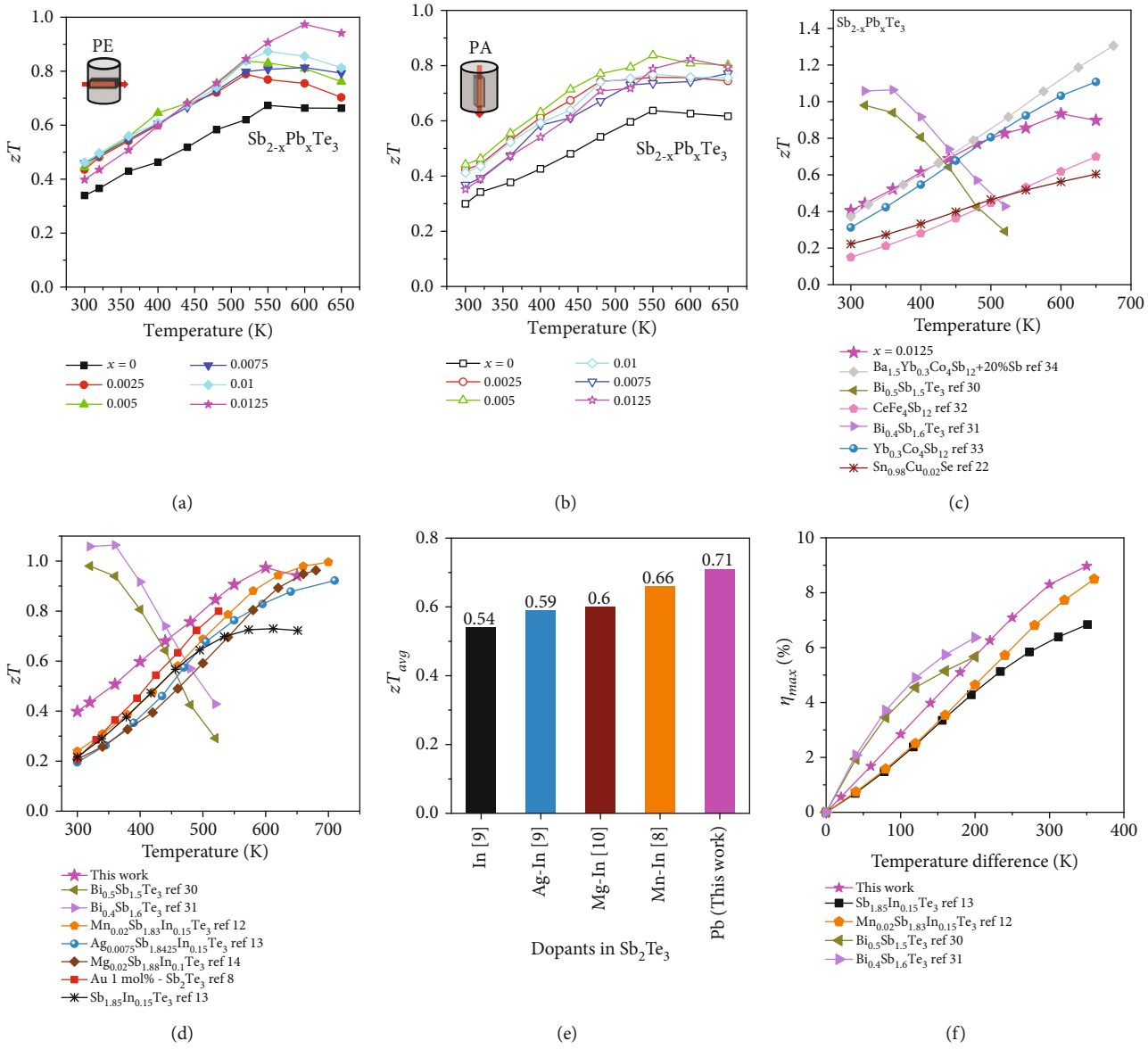


Figure 5: Thermoelectric performance of the $Sb_{2-x}Pb_xTe_3$ samples. $zT$ as a function of temperature along (a) PE and (b) PA directions. Comparison of the thermoelectric performances of $Sb_{1.9875}Pb_{0.0125}Te_3$ and other thermoelectric alloys [8–10, 18, 29–31, 33, 34]: (c, d) $zT$, (e) $zT_{avg}$, and (f) $\eta_{max}$.

is the Lorenz number). $L$ can be calculated using the following equation [29]:

$$L = 1.5 + \exp\left(\frac{|S|}{116}\right)\left(10^{-8}\mathrm{W\Omega/K^{-2}}\right) \quad (4)$$

Figures 4(b) and 4(d) show $\kappa_{latt}$ as a function of temperature along the PE and PA directions, respectively, which was calculated by subtracting $\kappa_{elec}$ from $\kappa_{tot}$. $\kappa_{latt}$ decreased with $x$ owing to an increase in the point defect phonon scattering by the $Pb^{2+}$ ions. The $\kappa_{latt}$ for high-doped samples for $x =$ 0.01 and 0.0012 for the PE direction was calculated very low, but this seems to be due the error in the $L$ calculation, which can be expected from the error in $L$ for very high conductive alloys ($\sigma > 3000$ S/cm) [25]. (See Figure S5 in Supplementary Materials for thermal transport properties of the highly doped $Sb_{2-x}Pb_xTe_3$ samples along the PE direction.)

Figures 5(a) and 5(b) show the $zT$ of the $Sb_{2-x}Pb_xTe_3$ samples as a function of temperature along the PE and PA directions, respectively. A maximum $zT$ or $zT_{max}$ of 0.97 was obtained for $x = 0.0125$ at 600 K along the PE direction, which is approximately 45% higher than that of pristine $Sb_2Te_3$ ($zT_{max} \sim 0.67$ at 550 K). A $zT_{max}$ of 0.84 was obtained for $x = 0.005$ at 550 K along the PA direction, which is 33% higher than that of pristine $Sb_2Te_3$ ($zT_{max} \sim 0.64$ at 550 K). (See Figure S6 in Supplementary Materials for $zT$ of the highly doped $Sb_{2-x}Pb_xTe_3$ samples.)

Figure 5(c) compares the $zT$ values of $Sb_{1.9875}Pb_{0.0125}Te_3$ (i.e., $x = 0.0125$) and several high-performance thermoelectric

alloys in the midtemperature (namely, $CeFe_4Sb_{12}$, $Yb_{0.3}Co_4Sb_{12}$, and $Sn_{0.098}Cu_{0.02}Se$) and near-room temperature (namely, $p$-type $Bi_{0.5}Sb_{1.5}Te_3$ and $Bi_{0.4}Sb_{1.6}Te_3$) range [30–34]. The $zT$ values of $Sb_{1.9875}Pb_{0.0125}Te_3$ in this temperature range were comparable to those of filled skutterudites such as $XFe_3Sb_{12}$ and $XCo_3Sb_{12}$ (where $X$ = Yb, Ce, In, etc.), which require a complex and lengthy synthesis process [32–34]. In addition, the $zT$ values of $Sb_{1.9875}Pb_{0.0125}Te_3$ were comparable to those of $Sb_2Te_3$ alloys codoped with In (Figure 5(d)). Furthermore, the $zT$ values of $Sb_{1.9875}Pb_{0.0125}Te_3$ were much higher than those of codoped $Sb_2Te_3$ alloys in the temperature range 300–600 K. Consequently, the $zT_{avg}$ of $Sb_{1.9875}Pb_{0.0125}Te_3$ was 0.71, which is higher than that of the codoped $Sb_2Te_3$ alloys (Figure 5(e)).

Figure 5(f) compares the $\eta_{max}$ values of $Sb_{1.9875}Pb_{0.0125}Te_3$ and other alloys. A $\eta_{max}$ of 9.0% was obtained for $Sb_{1.9875}Pb_{0.0125}Te_3$ corresponding to a temperature difference of 350 K, which was calculated using Eq. (1). This is 32% higher than that of singly doped $Sb_{1.85}In_{0.15}Te_3$ ($\eta_{max}$ = 6.8%) [13]. Moreover, although $Mn_{0.02}Sb_{1.83}In_{0.15}Te_3$ ($\eta_{max}$ = 8.5%) exhibited the highest $zT$ [12], $\eta_{max}$ of $Sb_{1.9875}Pb_{0.0125}Te_3$ exceeded that of $Mn_{0.02}Sb_{1.83}In_{0.15}Te_3$. The singly and lightly Pb-doped $Sb_2Te_3$ could outperform other singly or codoped $Sb_2Te_3$ with respect to power generation in midtemperature range.

## 4. Conclusion

In this study, we synthesized a series of polycrystalline bulk $Sb_{2-x}Pb_xTe_3$ (with $x$ = 0, 0.0025, 0.005, 0.0075, 0.01, and 0.0125) samples using the traditional solid-state reaction method. The electrical conductivity of the samples increased from 2,240 S/cm for pristine $Sb_2Te_3$ to 3,570 S/cm with Pb doping. However, the Seebeck coefficient of the samples was not affected significantly by the improved effective mass. An optimal power factor of 3.7 mW/mK$^2$ was obtained at 300 K for $x$ = 0.01, which is 39% higher than that of the pristine sample (2.6 mW/mK$^2$). The lattice thermal conductivity of the Pb-doped samples decreased significantly with the doping content owing to an increase in point defect phonon scattering. Consequently, a maximum $zT$ value of 0.97 was obtained for $x$ = 0.0125, which is 45% higher than that of pristine $Sb_2Te_3$. We also compared the performance of the $Sb_{2-x}Pb_xTe_3$ alloys developed in this work with that of other high-efficiency thermoelectric alloys in the midtemperature range, including filled skutterudites and codoped $Sb_2Te_3$ alloys.

## Data Availability

Data are available upon reasonable request.

## Conflicts of Interest

The authors declare that they have no competing interests.

## Authors' Contributions

Okmin Park and Kyu Hyoung Lee contributed equally to this work.

## Acknowledgments

This study was supported by the Nano·Material Technology Development Program under the National Research Foundation of Korea (NRF) funded by the Ministry of Science and ICT (2022M3H4A1A04076667).

## Supplementary Materials

The energy-dispersive spectroscopy (Quantax Xflash 6-60, Bruker, USA) by scanning electron microscope (SU8010, HITACHI, Japan) is measured to confirm the doping for the samples. Table S1: atomic percentage in $Sb_{2-x}Pb_xTe_3$ samples obtained from energy-dispersive spectroscopy (EDS). Figure S1: EDS mapping images of $Sb_{2-x}Pb_xTe_3$ samples ($x$ = 0, 0.0025, 0.005, 0.075, 0.01, and 0.0125). The higher doping of Pb in $Sb_{2-x}Pb_xTe_3$ beyond $x$ = 0.0125 was investigated by introducing large amounts of Pb corresponding to $x$ = 0.05, 0.1, 0.15, and 0.2, and the results are shown in Supplementary Materials. Figure S2: (a) XRD patterns and (b) lattice parameters of the highly doped $Sb_{2-x}Pb_xTe_3$ samples. Figure S3: thermoelectric transport properties of the highly doped $Sb_{2-x}Pb_xTe_3$ samples along the PE direction: (a) electrical conductivity, (b) Seebeck coefficient, and (c) power factor as functions of temperature. Figure S4: carrier transport properties of the highly doped $Sb_{2-x}Pb_xTe_3$ samples along the PE direction: (a) Hall carrier concentration, (b) Hall mobility, and (c) DOS effective mass, as functions of the doping content. (d) Logarithmic carrier concentration as a function of the absolute Seebeck coefficient. Figure S5: thermal transport properties of the highly doped $Sb_{2-x}Pb_xTe_3$ samples along the PE direction. (a) Total and (b) lattice thermal conductivity, as functions of temperature. The inset in (a) shows the electron thermal conductivity as a function of temperature. Figure S6: (a) thermoelectric figure of merit and (b) weighted mobility of the highly doped $Sb_{2-x}Pb_xTe_3$ samples, as functions of temperature. *(Supplementary Materials)*

## References

[1] Z. H. Zheng, X. L. Shi, D. W. Ao et al., "Harvesting waste heat with flexible Bi2Te3 thermoelectric thin film," *Nature Sustainability*, vol. 6, no. 2, pp. 180–191, 2023.

[2] B. Hu, X. L. Shi, J. Zou, and Z. G. Chen, "Thermoelectrics for medical applications: progress, challenges, and perspectives," *Chemical Engineering Journal*, vol. 437, article 135268, 2022.

[3] X. L. Shi, W. D. Liu, M. Li et al., "A solvothermal synthetic environmental design for high-performance SnSe-based thermoelectric materials," *Advanced Energy Materials*, vol. 12, no. 20, article 2200670, 2022.

[4] Z. Miao, X. Meng, and L. Liu, "Improving the ability of thermoelectric generators to absorb industrial waste heat through three-dimensional structure optimization," *Applied Thermal Engineering*, vol. 228, article 120480, 2023.

[5] Y. Yu, D. S. He, S. Zhang et al., "Simultaneous optimization of electrical and thermal transport properties of $Bi_{0.5}Sb_{1.5}Te_3$ thermoelectric alloy by twin boundary engineering," *Nano Energy*, vol. 37, pp. 203–213, 2017.

[6] S. I. Kim, K. H. Lee, H. A. Mun et al., "Dense dislocation arrays embedded in grain boundaries for high-performance bulk thermoelectrics," *Science*, vol. 348, no. 6230, pp. 109–114, 2015.

[7] B. Poudel, Q. Hao, Y. Ma et al., "High-thermoelectric performance of nanostructured bismuth antimony telluride bulk alloys," *Science*, vol. 320, no. 5876, pp. 634–638, 2008.

[8] W. Zheng, Y. Luo, Y. Liu, J. Shi, R. Xiong, and Z. Wang, "Synergistical tuning interface barrier and phonon propagation in Au–$Sb_2Te_3$ nanoplate for boosting thermoelectric performance," *Journal of Physical Chemistry Letters*, vol. 10, no. 17, pp. 4903–4909, 2019.

[9] J. Wang, C. Zhou, Y. Yu et al., "Enhancing thermoelectric performance of $Sb_2Te_3$ through swapped bilayer defects," *Nano Energy*, vol. 79, article 105484, 2021.

[10] P. K. Nguyen, K. H. Lee, J. Moon et al., "Spark erosion: a high production rate method for producing Bi0.5Sb1.5Te3nanoparticles with enhanced thermoelectric performance," *Nanotechnology*, vol. 23, no. 41, article 415604, 2012.

[11] H. Qin, J. Zhu, N. Li et al., "Enhanced mechanical and thermoelectric properties enabled by hierarchical structure in medium-temperature $Sb_2Te_3$ based alloys," *Nano Energy*, vol. 78, article 105228, 2020.

[12] H. Qin, J. Zhu, B. Cui et al., "Achieving a high average zT value in $Sb_2Te_3$-based segmented thermoelectric materials," *ACS Applied Materials & Interfaces*, vol. 12, no. 1, pp. 945–952, 2020.

[13] L. P. Hu, T. J. Zhu, X. Q. Yue et al., "Enhanced figure of merit in antimony telluride thermoelectric materials by In-Ag co-alloying for mid-temperature power generation," *Acta Materialia*, vol. 85, pp. 270–278, 2015.

[14] L. Xie, H. Qin, J. Zhu et al., "Realizing excellent thermoelectric performance of $Sb_2Te_3$ based segmented leg with a wide temperature range using one-step sintering," *Advanced Electronic Materials*, vol. 6, no. 2, article 1901178, 2020.

[15] R. J. Mehta, Y. Zhang, H. Zhu et al., "Seebeck and figure of merit enhancement in nanostructured antimony telluride by antisite defect suppression through sulfur doping," *Nano Letters*, vol. 12, no. 9, pp. 4523–4529, 2012.

[16] M. Wei, X.-L. Shi, Z.-H. Zheng et al., "Directional thermal diffusion realizing inorganic $Sb_2Te_3$/Te hybrid thin films with high thermoelectric performance and flexibility," *Advanced Functional Materials*, vol. 32, no. 45, article 2207903, 2022.

[17] J.-E. Hong, S.-K. Lee, and S.-G. Yoon, "Enhanced thermoelectric properties of thermal treated $Sb_2Te_3$ thin films," *Journal of Alloys and Compounds*, vol. 583, pp. 111–115, 2014.

[18] M. Wei, T.-B. Chen, J.-G. Hu et al., "Effect of organic nanocomponents on the thermoelectric properties of $Sb_2Te_3$ nanocrystal thin film," *Scripta Materialia*, vol. 185, pp. 105–110, 2020.

[19] G. Thankamma and A. G. Kunjomana, "Enhancement of thermoelectric efficiency in vapor deposited $_{Sb2Te3and}$ Sb1.8In0.2-Te3crystals," *Crystal Research and Technology*, vol. 49, no. 4, pp. 212–219, 2014.

[20] H.-S. Kim, K. H. Lee, J. Yoo et al., "Effect of substitutional Pb doping on bipolar and lattice thermal conductivity in p-type $Bi_{0.48}Sb_{1.52}Te_3$," *Materials*, vol. 10, no. 7, p. 763, 2017.

[21] M.-K. Han, X. Zhou, C. Uher, S.-J. Kim, and M. G. Kanatzidis, "Increase in the figure of merit by Cd-substitution in $Sn_{1-x}Pb_xTe$ and effect of Pb/Sn ratio on thermoelectric properties," *Advanced Energy Materials*, vol. 2, no. 10, pp. 1218–1225, 2012.

[22] N. K. Singh, S. Bathula, B. Gahtori, K. Tyagi, D. Haranath, and A. Dhar, "The effect of doping on thermoelectric performance of p-type SnSe: promising thermoelectric material," *Journal of Alloys and Compounds*, vol. 668, pp. 152–158, 2016.

[23] A. S. Pashinkin, A. S. Malkova, and M. S. Mikhailova, "The heat capacity of solid antimony telluride $Sb_2Te_3$," *Russian Journal of Physical Chemistry*, vol. 82, no. 5, pp. 878-879, 2008.

[24] K. Ahmad, Z. Almutairi, and C. Wan, "Thermoelectric properties of PbTe-based graphene nanocomposite," *Journal of Materials Science: Materials in Electronics*, vol. 31, no. 23, pp. 20996–21004, 2020.

[25] K. Zhang, H. Wang, W. Su et al., "Trace bismuth and iodine co-doping enhanced thermoelectric performance of PbTe alloys," *Journal of Physics D: Applied Physics*, vol. 53, no. 24, p. 245501, 2020.

[26] G. J. Snyder, A. H. Snyder, M. Wood, R. Gurunathan, B. H. Snyder, and C. Niu, "Weighted mobility," *Advanced Materials*, vol. 32, no. 25, p. 2001537, 2020.

[27] K. H. Lee, S.-I. Kim, J.-C. Lim, J. Y. Cho, H. Yang, and H.-S. Kim, "Approach to determine the density-of-states effective mass with carrier concentration-dependent Seebeck coefficient," *Advanced Functional Materials*, vol. 32, no. 33, article 2203852, 2022.

[28] L. Lorenz, "Bestimmung der Wärmegrade in absolutem Maasse," *Annalen der Physik und Chemie*, vol. 223, no. 11, pp. 429–452, 1872.

[29] H.-S. Kim, Z. M. Gibbs, Y. Tang, H. Wang, and G. J. Snyder, "Characterization of Lorenz number with Seebeck coefficient measurement," *APL Materials*, vol. 3, no. 4, article 041506, 2015.

[30] H. Li, X. Su, X. Tang et al., "Grain boundary engineering with nano-scale InSb producing high performance $In_xCe_yCo_4Sb_{12+z}$ skutterudite thermoelectrics," *Journal of Materiomics*, vol. 3, no. 4, pp. 273–279, 2017.

[31] G. Tan, W. Liu, S. Wang et al., "Rapid preparation of $CeFe_4Sb_{12}$ skutterudite by melt spinning: rich nanostructures and high thermoelectric performance," *Journal of Materials Chemistry A*, vol. 1, no. 40, pp. 12657–12668, 2013.

[32] D. Qin, B. Cui, X. Meng et al., "High thermoelectric performance from high carrier mobility and reduced lattice thermal conductivity in Ba, Yb double-filled skutterudites," *Materials Today Physics*, vol. 8, pp. 128–137, 2019.

[33] K.-H. Lee, H.-S. Kim, S.-I. Kim et al., "Enhancement of thermoelectric figure of merit for $Bi_{0.5}Sb_{1.5}Te_3$ by metal nanoparticle decoration," *Journal of Electronic Materials*, vol. 41, no. 6, pp. 1165–1169, 2012.

[34] K.-H. Lee, S. Hwang, B. Ryu et al., "Enhancement of the thermoelectric performance of $Bi_{0.4}Sb_{1.6}Te_3$, alloys by In and Ga doping," *Journal of Electronic Materials*, vol. 42, no. 7, pp. 1617–1621, 2013.